Monthly Notices of the ROYAL ASTRONOMICAL SOCIETY

MNRAS **543,** 223–232 (2025) https://doi.org/10.1093/mnras/staf1424
Advance Access publication 2025 September 18

Discovery of an icy and nitrogen-rich extrasolar planetesimal

Snehalata Sahu [1]★ Boris T. Gänsicke [1,2] Jamie T. Williams [1] Detlev G. Koester [3] Jay Farihi [4] Steven J. Desch,[5] Nicola Pietro Gentile Fusillo [6,7] Dimitri Veras [1,8,9] Sean N. Raymond [10] and Maria Teresa Belmonte[11]

[1]*Department of Physics, University of Warwick, Coventry, CV4 7AL, UK*
[2]*Instituto de Astrofísica de Canarias, La Laguna, Tenerife E-38205, Spain*
[3]*Institut für Theoretische Physik und Astrophysik, Christian-Albrechts-Universität, D-24118 Kiel, Germany*
[4]*Department of Physics and Astronomy, University College London, London, WC1E 6BT, UK*
[5]*School of Earth and Space Exploration, Arizona State University, PO Box 876004, Tempe, AZ 85287-6004, USA*
[6]*Department of Physics, Università degli Studi di Trieste, Via A. Valerio 2, I-34127 Trieste, Italy*
[7]*INAF – Osservatorio Astronomico di Trieste, via Tiepolo 11, I-34131 Trieste, Italy*
[8]*Centre for Exoplanets and Habitability, University of Warwick, Coventry, CV4 7AL, UK*
[9]*Centre for Space Domain Awareness, University of Warwick, Coventry, CV4 7AL, UK*
[10]*Laboratoire d'Astrophysique de Bordeaux, CNRS and Université de Bordeaux, Allée Geoffroy St. Hilaire, F-33165 Pessac, France*
[11]*Departamento de Física Teórica, Universidad de Valladolid, Atómica y Óptica, P.° de Belén, 7, Valladolid E-47011, Spain*

Accepted 2025 August 21. Received 2025 August 20; in original form 2025 June 25

ABSTRACT

White dwarfs accreting planetary debris provide detailed insight into the bulk composition of rocky exoplanetesimals. However, only one Kuiper Belt analogue has been identified in that way so far. Here, we report the accretion of an icy extrasolar planetesimal on to white dwarf WD 1647+375 using ultraviolet spectroscopy from the *Hubble Space Telescope*. The accreted material is rich in the volatiles carbon, nitrogen, and sulphur, with a chemical composition analogous to Kuiper belt objects (KBOs) in our Solar system. It has a high nitrogen mass fraction (5.1 ± 1.6 per cent) and large oxygen excess (84 ± 7 per cent), indicating that the accreted planetesimal is water-rich (a water-to-rock ratio of ≃2.45), corroborating a cometary- or dwarf planet-like composition. The white dwarf has been accreting at a rate of $\approx 2 \times 10^8$ g s^{-1} for the past 13 yrs, implying a minimum mass of $\sim 10^{17}$ g for the icy parent body. The actual mass could be several orders of magnitude larger if the accretion phase lasts $\sim 10^5$ yr as estimated in the literature from debris disc studies. We argue that the accreted body is most likely a fragment of a KBO dwarf planet based on its nitrogen-rich composition. However, based on the chemical composition alone, it is difficult to discern whether this icy body is intrinsic to this planetary system, or may have an interstellar origin.

Key words: techniques: spectroscopic – exoplanets – planets and satellites: composition – white dwarfs – ultraviolet: stars.

1 INTRODUCTION

The Solar system contains a vast number of icy bodies, including comets and the moons of giant planets. These bodies originate in distant regions of the Solar system, such as the Kuiper belt and the Oort cloud, where temperatures are sufficiently low for volatile ices to remain in solid form. These objects are predominantly composed of water, CO_2, and NH_3, and are representative of the primitive and unaltered matter from the early solar nebula. They offer key insights into the composition of protoplanetary discs and thus are important for understanding the delivery of water (and potentially the origins of life Anders 1989; Anslow, Bonsor & Rimmer 2023) on to terrestrial planets. The source of water on Earth remains an intensively debated topic (see e.g. Piani et al. 2020; Kral et al. 2024; Barrett, Bryson & Geraki 2025), where a few recent studies suggest that water could be produced by the chemical reactions of primordial hydrogen-dominated atmospheres with magma oceans (Young, Shahar & Schlichting 2023; Rogers et al. 2025).

Beyond the Solar system, a small number of exo-comets (see the review by Strøm et al. 2020) have been discovered via high-resolution spectra of transient absorption features (such as Ca II, Fe II) caused by the dusty tails of comets while transiting the star (Kiefer et al. 2014a, b; Welsh & Montgomery 2018). These observations are challenging, as these icy exoplanetary bodies are small and faint. Since typically only gases are detected, our insight into the detailed chemical composition of the exo-comets remains limited. In this respect, white dwarfs have the potential to serve as powerful diagnostic tools for investigating the bulk composition of exoplanetary icy bodies.

White dwarfs with $T_{\rm eff} < 25\,000$ K typically have simple atmospheres dominated by hydrogen or helium, as heavy elements formed during earlier evolutionary stages sink to the core under the influence of their high surface gravities (Schatzman 1945). The sinking timescales for these metals are always short (ranging from days to millions of years, depending on whether the atmosphere is dominated by H or

★ E-mail: snehalatash30@gmail.com

He, (see Koester 2009) compared to the time the star has spent in the white dwarf phase. The detection of metals in their atmospheres is therefore attributed to external sources, primarily from the accretion of planetary debris (Jura 2003), as confirmed by many studies in the past two decades (Farihi et al. 2010; Klein et al. 2010; Kawka & Vennes 2012; Hollands et al. 2017; Izquierdo et al. 2021). This phenomenon makes them powerful probes of the bulk composition of exoplanetary bodies (Zuckerman et al. 2007).

Optical and ultraviolet spectroscopic surveys have shown that between 25 per cent (Zuckerman et al. 2003) to 50 per cent (Koester, Gänsicke & Farihi 2014) of white dwarfs exhibit photospheric metals. Among the heavy elements, O, Mg, Si, Ca, and Fe are typically the most abundant, consistent with the accretion of rocky bodies. Detailed analyses of a small number of heavily metal-enriched white dwarfs have revealed abundance patterns that closely resemble those of bulk Earth or CI chondrites (Gänsicke et al. 2012; Melis & Dufour 2017; Doyle et al. 2023). In contrast, only a handful of systems have been found accreting volatile-rich material containing elements such as C, N, S, or excess oxygen that is indicative of water-rich bodies (Farihi, Gänsicke & Koester 2013; Raddi et al. 2015; Gentile Fusillo et al. 2017; Xu et al. 2017).

Given the ubiquity of icy bodies in our Solar system, the observational findings discussed above raise an important question: Why is the detection of white dwarfs accreting volatile-rich material so rare? Whereas comets and Kuiper belt-like objects are numerous in the Solar system, and very likely also in exoplanetary systems, a large fraction of them are likely to be ejected during the metamorphosis of their host stars into white dwarfs (Veras, Shannon & Gänsicke 2014a; Stone, Metzger & Loeb 2015). In addition, there is a strong observational selection effect: cool white dwarfs (<13 000 K) usually dominate the spectroscopic surveys which are less sensitive to detecting volatiles (such as C, N, O) due to their weaker transitions in optical wavelengths (Williams et al. 2024). Furthermore, recent studies have highlighted other possible explanations, including observational biases due to asynchronous accretion (Malamud & Perets 2016; Brouwers et al. 2023), and the shielding effect of white dwarf magnetospheres, which can prevent the accretion of volatile vapours (produced by sublimating comet fragments) within the co-rotation radius (Zhou, Liu & Lin 2024).

To identify and characterize the volatile-enriched white dwarf systems, measuring the abundance of nitrogen is crucial as it serves as a key indicator of exoplanetary ices or primitive material enriched with volatile elements, similar to those found in comets, interstellar objects (Oumuamua Jackson & Desch 2021), Kuiper Belt objects (KBOs), and the crusts of icy moons of the outer Solar system. The detection of nitrogen requires far-ultraviolet spectroscopy, and has so far only been reported for three of the white dwarfs with He (Xu et al. 2017; Klein et al. 2021) and H-rich atmospheres (Johnson et al. 2022). The overall chemical composition of the debris accreted by these three white dwarfs indicates that they accreted Kuiper belt-like objects.

Here, we report nitrogen detection in a warm (22 040 K) hydrogen-rich atmosphere of WD 1647+375 using far-ultraviolet spectroscopy obtained with *Hubble Space Telescope* (*HST*). In addition to nitrogen, we detect other volatile elements (C, O, S) which, combined with its large oxygen excess, imply that this white dwarf is accreting an icy exoplanetesimal.

2 OBSERVATION AND DATA ANALYSIS

We obtained ultraviolet and optical spectroscopy to measure the metal abundances in the atmosphere of WD 1647+375. Below, we provide details on these observations and describe the fitting technique as well as the computation of the accretion rates calculated from the best-fitting abundances.

Table 1. Comparison of line velocities derived from two COS observing programmes of WD 1647+375 with exposure times of 780 s (snapshot) and 2164 s (deep).

Metal	Wavelength region (Å)	V_r (km s^{-1}) Snapshot	Deep
C III	1175–1177	14.37 ± 0.55	13.04 ± 0.36
C II[a]	1334–1335	12.24 ± 0.38	13.74 ± 0.26
N I[a]	1199–1200	14.84 ± 6.18	7.18 ± 2.75
N I	1242–1245	15.29 ± 3.59	1.42 ± 2.81
O I	1151–1153	18.40 ± 0.93	13.01 ± 0.64
O I[a]	1302–1306	19.75 ± 0.38	19.1 ± 0.23
Al III	1379–1384	12.67 ± 1.05	12.39 ± 0.69
Si II	1260–1265	18.41 ± 0.29	10.95 ± 0.19
Si III[a]	1298–1301	20.10 ± 0.26	17.92 ± 0.18

[a]These photospheric features are contaminated by lines from the interstellar medium (ISM).

2.1 Ultraviolet spectroscopy

WD 1647+375 was observed twice with the Cosmic Origins Spectrograph (COS) onboard *HST*. An initial observation with an exposure time of 780 s was obtained on 2011 October 5 as part of the snapshot programme 12474, followed by a deep exposure using a 2164 s integration on 2012 December 16 under programme 12 869 (PI Boris Gänsicke for both programmes). On both occasions, we used the G130M grating with a central wavelength of 1291 Å which covers the wavelength range 1130−1435 Å, with a gap at 1278−1288 Å due the space between two detector segments. The resolving power of the grating is $R = 16\,000$. The spectra were processed with the COS pipeline CALCOS 3.1.8.

The snapshot spectrum was acquired with the lifetime position LP1, and the deeper exposure spectrum at LP2. Since the COS wavelength accuracy corresponds to a velocity of 15 km s^{-1}, we used the spectra of WD 1647+375 to check for differences between the measurements arising from the wavelength calibration in different LP settings. Comparing line velocities, we find that there is an average velocity offset of ≈10–12 km s^{-1} between the N I 1243 Å doublet and other strong absorption lines of C, Si, and O within the deep exposure. In contrast, all line velocities are consistent in the case of snapshot spectrum (Table 1). Inspecting the two COS spectra, we find a relative shift in the wavelength calibration of deep exposure (≈0.04 Å), particularly in the 1200–1300 Å spectral region. This velocity difference may arise due to an error in COS wavelength calibration, which depends on wavelength accuracy, geometric distortions, and drifts (Oliverira et al. 2010).

The O I triplet (1302–1306 Å) in the spectra can be affected by the geocoronal lines whose intensity varies as a function of *HST*'s orbital position (i.e. the observatory's 'day' and 'night' time). Both *HST* spectra of WD 1647+675 are strongly affected by airglow. We used community-generated templates for COS (Bourrier et al. 2018) to remove this feature from the spectra (Williams et al. 2025) as shown in Fig. 1. The corrected spectra for both exposures were used for determining the oxygen abundance.

2.2 Optical spectroscopy

A low resolution ($R \approx 1000$) spectrum of WD 1647+375 obtained by Gianninas, Bergeron & Ruiz (2011) is available in the Montreal

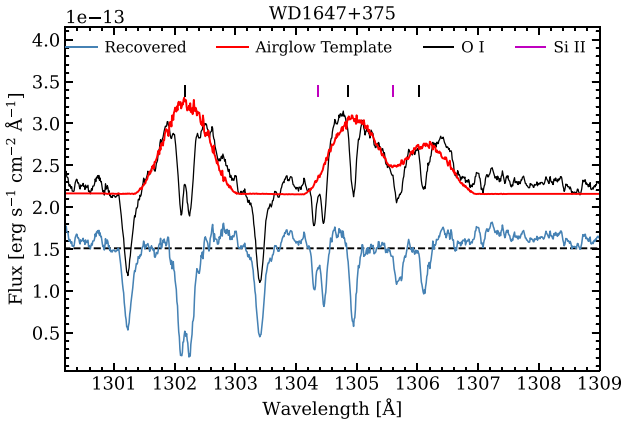

Figure 1. Airglow correction of WD 1647+375 of the deep exposure where the raw spectrum and the best-fitting airglow template are shown in black and red, respectively. The airglow-corrected spectrum is shown in blue and arbitrarily shifted in flux for clarity. The strong absorption lines of Si II and O I affected by the airglow are marked in the plot. The dashed black line shows the average continuum flux in the wavelength region 1300–1309 Å.

Table 2. Summary of parameters for WD 1647+375.

Parameters	Value
Name	WD J164920.30+372821.25
G (mag)	14.986 (0.003)
Parallax (mas)	12.74 (0.03)
$T_{\rm eff}$ (K)	22 040 (31)
log (g[cm s^{-2}])	7.88 (0.03)
M ($M_\odot$)	0.57 (0.01)
R ($R_\odot$)	0.0144 (0.0003)
Cooling age (Myr)	30 (2)

Note. Astrometric parameters are from Gaia Collaboration (2023) and spectroscopic parameters are from Sahu et al. (2023).

White Dwarf Data Base (Dufour et al. 2017), which does not exhibit any metal lines. A more recent spectrum ($R \simeq 2500$) was obtained as part of the Data Release 1 of the Dark Energy Spectroscopic Instrument (DESI Collaboration 2025), again not showing any metal lines.

We therefore observed WD 1647+375 on 2025 April 23 with the X-shooter spectrograph (Vernet et al. 2011) mounted on the Very large Telescope (VLT), using slit widths of 1.0, 0.9, and 0.9 arcsec and exposure times of 2 × 200 s, 2 × 150 s, and 4 × 100 s in the UVB, VIS, and NIR arms, respectively. The resulting spectral resolutions are 5400 (UVB), 8900 (VIS), and 5600 (NIR). The data were reduced using the REFLEX pipeline and the telluric correction was carried out using MOLECFIT (Kausch et al. 2015). The only metal absorption line detected in the X-Shooter spectrum is the Mg II triplet at 4481 Å.

2.3 Metal abundances

WD 1647+375 has $T_{\rm eff} = 22\,040$ K, $\log g = 7.88$, and a hydrogen-dominated atmosphere (Table 2; Sahu et al. 2023). Fixing these parameters, we generated 1D synthetic spectral model grids for the elements C, N, O, Mg, Al, Si, P, S, Ca, Fe, and Ni using the atmosphere code of Koester (2010) but with numerous updates and improvements in the equations of state and absorption coefficients (Koester, Kepler & Irwin 2020). The model grids span abundances from −10 to −4 dex in steps of 0.25 dex. The analysis of the COS and X-Shooter spectroscopy of WD 1647+375 followed the methodology described in Williams et al. (2025).

Since WD 1647+375 is located at a distance of 78.5 pc (Table 2; Gaia Collaboration 2023), some of the photospheric lines in the COS spectrum are contaminated by absorption lines arising from the ISM, affecting the abundance measurements. We therefore included ISM lines in the fits to the COS spectrum, where each ISM line was modelled with a Gaussian profile using velocity, amplitude, and width as free parameters. The model ISM lines were then combined with the atmospheric model, convolved with the COS line spread function,[1] and fitted to the observed spectra using χ^2 minimization. In these fits, we used a spectral window of 3 Å centred around the vacuum (COS) and air (X-Shooter) wavelengths of the detected metal lines, and allowed for a local flux scaling factor to match the continua of the data and the model.

In addition to the ISM lines, the spectral region 1290–1310 Å contains many strong photospheric Si II, III lines that affect the level of the continuum and thereby the oxygen abundance determination using O I 1302.17, 1304.86 and 1306.03 Å. To resolve this, we fixed the Si abundance to the initial best-fitting value and generated models varying each element relative to Si (one at a time) to find the best-fitting measurement. The difference between the abundance determined from the O I triplet and that from the unblended line at 1152 Å is comparable to the 1σ uncertainties noted in the case of other elements, suggesting that the measured oxygen abundance is reliable.

For nitrogen, we considered the spectral regions covering the N I triplet at 1200 Å and the doublet at 1243 Å which is a blend of four lines with the strongest transitions at 1243.18 and 1243.31 Å. We do not detect phosphorus or nickel absorption lines, hence, we determined upper limits considering the transitions P III 1344.33 Å, Ni II 1370.12 Å and following the procedure of Hollands et al. (2020). Fig. 2 shows the best-fitting model to the spectrum of WD 1647+375, where the determined abundances are given in Table 3. We note that the ISM lines are resolved from the photospheric lines with average line velocities of −19.5 and +11 km s^{-1}, respectively. We computed the final abundance values as the weighted average of the measurements derived from multiple lines of each element, and the uncertainties are adopted as the standard deviation for the COS spectrum.

We determined the best-fitting abundances for both COS spectra to (1) probe for temporal variations in the abundances, and (2) assess potential systematic uncertainties. The results are provided in Table 3. We find that the abundances agree well within the 1σ uncertainties for all elements. There is a difference of 0.14 dex in the oxygen abundance between the two COS spectra which is most likely related to the different levels of correction for airglow. Overall, the deeper exposure provides the best signal-to-noise ratio and thus the smallest uncertainties in detected lines (especially nitrogen, which has only weak lines) and tighter upper limits for non-detections. Hence, the abundance measurements of the deep spectrum were used to study the bulk composition of the accreted body. The results of the snapshot spectrum are provided in the Appendix A.

The snapshot exposure of WD 1647+375 has been previously analysed (Koester et al. 2014), yielding stellar parameters $T_{\rm eff} = 22803 \pm 310$ K, $\log g = 7.90 \pm 0.09$, $\log({\rm Si/H}) = -6.20 \pm 0.10$, and $\log({\rm C/H}) = -5.50 \pm 0.20$. We find Si and C abundances larger by 0.4 and 0.3 dex, respectively, which agree within 2σ with

[1] https://github.com/spacetelescope/notebooks/blob/master/notebooks/COS/LSF/LSF.ipynb

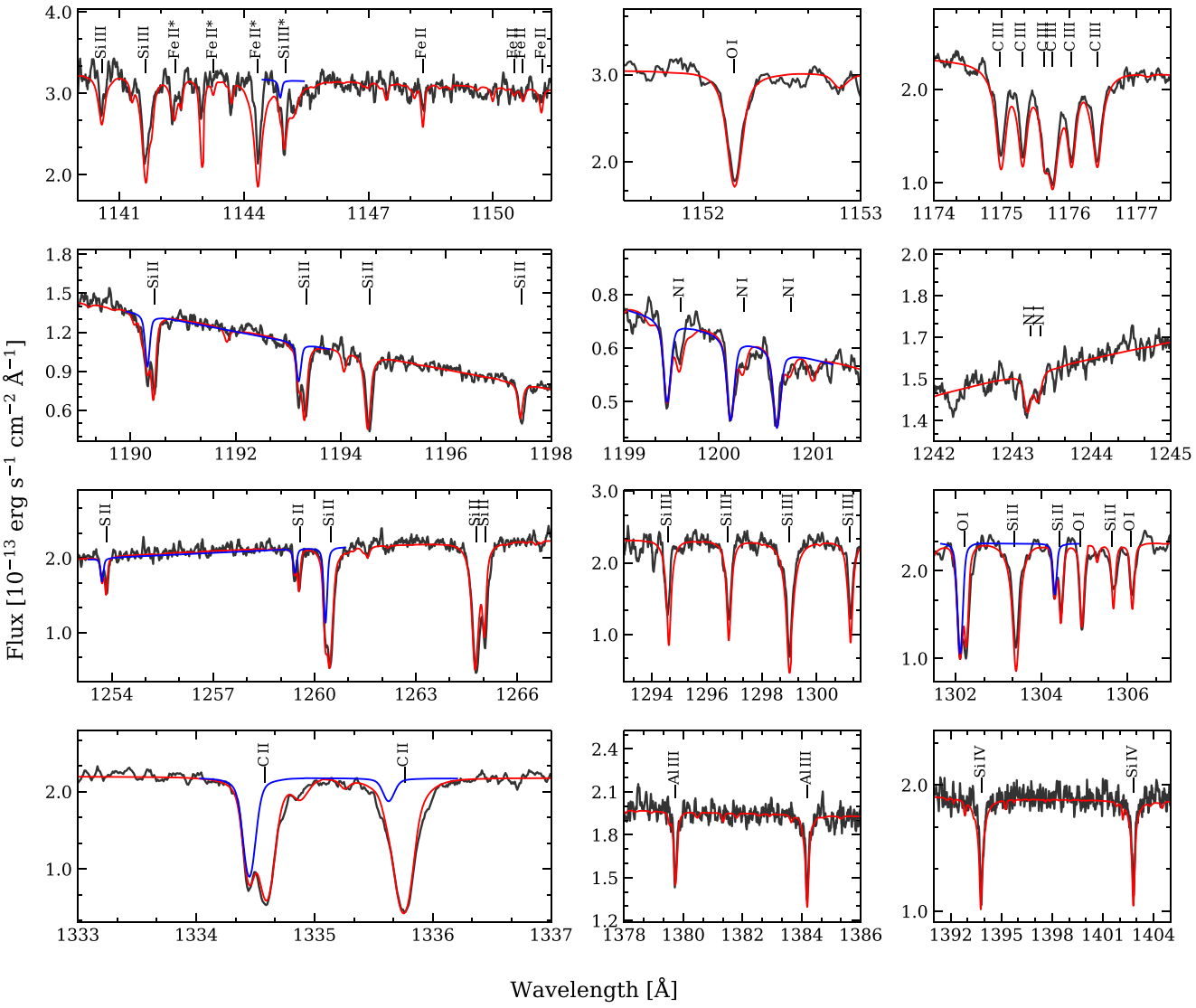

Figure 2. The airglow-corrected deep *HST* COS spectrum of WD 1647+375 (black) and the best-fitting model (red) with the line velocities from Table 1, and the weighted average abundances from Table 3. Since we have plotted the average abundances, the individual fits to the Si lines look poor. The ISM lines are fitted with a Gaussian profile and are shown in blue. Several transitions of C, N, O, S, Si, Al, and Fe are labelled, where ∗ denotes a blend of Si with Fe lines.

the earlier work. Using the deep exposure, Wilson et al. (2016) derived $\log(\mathrm{C/O}) = -1.12 \pm 0.25$, which is lower than our value of -0.50 ± 0.23. The abundance differences with these studies are attributed to the newer models, methods, and atomic data used in the current analysis.

The COS spectrum does not contain detectable transitions of magnesium and calcium, and we analysed the X-shooter spectrum to determine the abundances of these two elements. We fitted the spectral region covering the unresolved Mg II 4481 Å triplet, and Ca II K. We normalized the observed and model fluxes and varied the model abundances to find a best fit to the spectrum using χ^2 minimization. The X-Shooter spectrum and the best-fitting model for the Mg II are shown in Fig. 3, where we find a systemic velocity of $15.5 \pm 5.0\,\mathrm{km\,s^{-1}}$, consistent with the line velocities from COS. We do not detect Ca II absorption and hence we determined an upper limit as outlined above (Table 3).

2.4 Accretion rates

The bulk composition of the accreted material can be determined from the measured photospheric abundances by accounting for the different diffusion velocities of the individual elements. As the accreted material diffuses out of the warm and hydrogen-rich atmosphere of WD 1647+375 on time-scales of days (Koester 2009), it is safe to assume that there is a steady state between accretion and diffusion, and that the diffusion flux is constant throughout the atmosphere and is equal to the accretion rate, which in turn reflects the elemental composition of the parent body.

We computed the diffusion fluxes for each detected element following the procedure of Koester et al. (2014) which is applicable to warm, hydrogen-atmosphere white dwarfs with $T_{\rm eff} \geq 17\,000$ K. Note that the assumption of constant diffusion flux can lead to small changes in the photospheric abundances of the best-fitting model (Koester et al. 2014). We compared the spectrum emerging from an

Table 3. Summary of abundances of WD 1647+375. The abundances determined from the two COS spectra are reported separately.

Element	log (*Z*/*H*) Snapshot	log (*Z*/*H*) Deep	$\dot{M}_Z$ (g s^{-1})	Mass fraction (per cent) WD 1647+375	Mass fraction (per cent) Halley
		HST COS			
C	−5.22(0.15)	−5.18(0.21)	1.71×10^7	9.8 (4.6)	24.1
N	−5.66(0.29)	−5.68(0.12)	9.23×10^6	5.1 (1.6)	1.5
O	−4.83(0.04)	−4.69(0.10)	1.28×10^8	67.1 (6.6)	35.2
Al	−6.57(0.10)	−6.56(0.10)	1.35×10^6	0.7 (0.2)	0.5
Si	−5.76(0.29)	−5.74(0.21)	1.01×10^7	5.9 (2.9)	12.8
P	< −7.59	< −7.80	$< 1.17 \times 10^5$		
S	−6.32(0.12)	−6.30(0.10)	5.01×10^6	2.7 (0.8)	5.7
Fe	−6.20(0.15)	−6.20(0.13)	1.28×10^7	7.0 (2.3)	7.2
Ni	< −7.11	< −7.56	$< 6.45 \times 10^5$		0.6
		X-shooter			
Mg	−6.12 (0.14)		2.99×10^6	1.6 (0.5)	6.0
Ca	< −7.13		$< 7.78 \times 10^5$		0.6
Total			1.88×10^8		

Note. The error in magnesium abundance is adopted from Williams et al. (2024). The accretion rates and mass fraction are computed using the deep exposure spectra (exposure 2). The mass fraction of heavy elements in Halley's comet (Jessberger, Christoforidis & Kissel 1988) is provided for comparison.

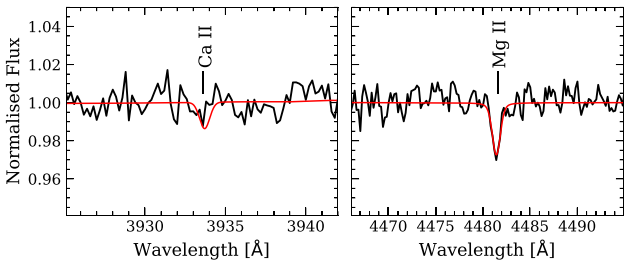

Figure 3. X-shooter spectrum of WD 1647+375 (black) and the best-fitting model (red) with an upper limit of log(Ca/H) (left panel) and log(Mg/H) (right panel) abundance from Table 3.

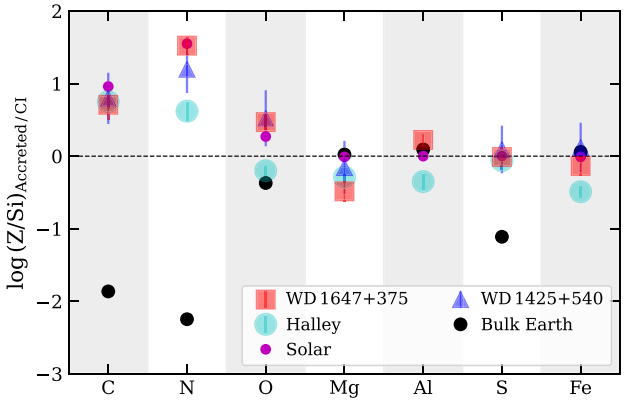

Figure 4. Comparison of log number abundance ratios of WD 1647+375, relative to silicon and normalized to CI chondrites, with the bulk Earth, Halley's comet (Jessberger et al. 1988) and WD 1425+540 (Model 1 from Xu et al. 2017).

atmosphere with a constant abundance and a constant diffusion flux, and found no noticeable difference. In addition, we assessed whether radiative levitation may affect the measured abundances. For the $T_{\rm eff}$ and log g of WD 1643+375, the study by Koester et al. (2014; fig. 5 and 6) suggests that the effect of radiative levitation is small. We verified this by computing an atmosphere model including radiative levitation for silicon and carbon following the procedures in Koester et al. (2014), and found that the implied changes in the diffusion fluxes are well below the 1σ uncertainties in the measurements. The accretion rates for each element are provided in Table 3.

3 RESULTS AND DISCUSSION

Whereas wind-accretion from a close stellar or substellar companion could explain the volatile-rich nature of the material accreted by WD 1647+375 (Debes 2006), we rule out that scenario for two reasons: (1) *Spitzer* photometry of WD 1647+375 does not reveal any infrared excess (Wilson et al. 2019). (2) Nitrogen is overabundant compared to solar abundances. For example, Gänsicke et al. (2012) reported COS spectroscopy of three white dwarfs accreting stellar wind from M-dwarf companions and found that the abundances of carbon, oxygen, and sulphur are quasi-solar, with nitrogen remaining below the detection threshold. Mass-loss from sub-stellar companions are expected to be extremely low, with only one optical detection (Walters et al. 2023). This leaves us with the accretion of planetary material as the only option. Below we discuss the composition of the planetary body, as well as its potential nature and origin.

3.1 The composition of the planetary body

We compared the parent body number abundances (see equation 2 of Gänsicke et al. 2012) derived from spectroscopy, relative to silicon and normalized to CI chondrites with the abundances of the bulk Earth (McDonough & Sun 1995), comet Halley (Jessberger et al. 1988); the Sun (Lodders 2003), and WD 1425+540 (Xu et al. (2017); the first case of volatile-dominated material detected in a polluted white dwarf) as shown in Fig. 4. This comparison suggests that the parent body accreted by WD 1647+375 closely resembles solar composition, Halley's comet, and the parent body polluting WD 1425+540. Notably, the accreted planetesimal is rich in carbon,

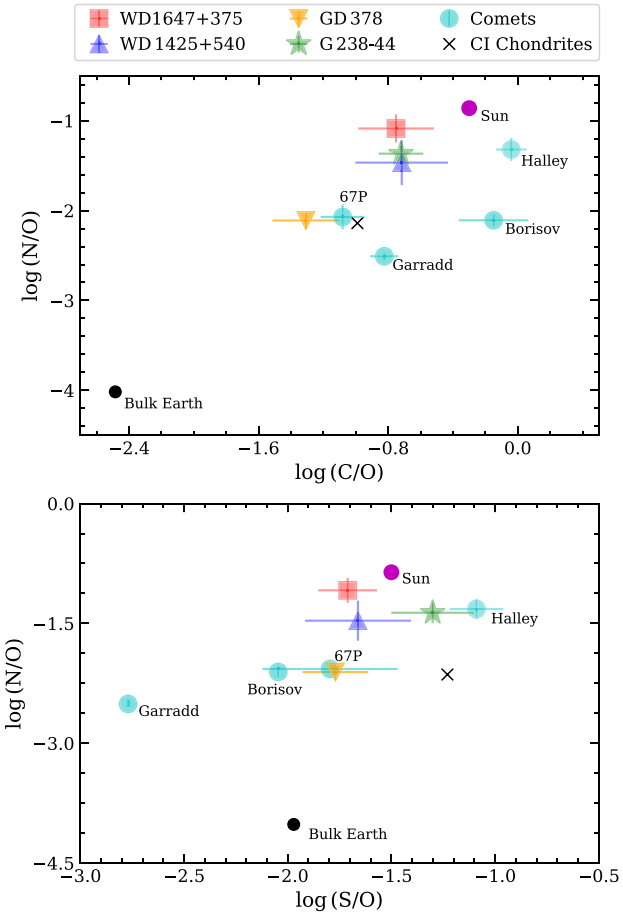

Figure 5. Log number abundance ratios of the volatiles carbon, nitrogen, and sulphur relative to oxygen in WD 1647+375 (red square) compared with the other three white dwarfs that have nitrogen detections (WD 1425+540 = blue triangle, Xu et al. 2017; GD 378 = yellow triangle, Klein et al. 2021; G 238−44 = green star, Johnson et al. 2022), and with well-studied comets (cyan): Halley; 67P/Churyumov-Gerasimenko (Rubin et al. 2019), Garradd (Paganini et al. 2012), 2I/Borisov (Bodewits et al. 2020), CI chondrites, Sun (Lodders 2003), and, bulk Earth (McDonough & Sun 1995). Note that 2I/Borisov is an interstellar comet.

oxygen, and nitrogen, with O/Si and N/Si being ∼5 and 8 times higher, respectively than the comet Halley. We further compared the volatile element ratios N/O, C/O, and S/O in Fig. 5, alongside Solar system and interstellar comets (Paganini et al. 2012; Rubin et al. 2019; Bodewits et al. 2020), and the three white dwarfs with photospheric nitrogen detections: WD 1425+540, G238−44, and GD 378. Fig. 5 places WD 1647+375 closer to the Sun in N/O than to the other, volatile-rich white dwarfs. WD 1647+375 exhibits N/O = 0.08, which is higher than in comets, which have N/O between 0.003 and 0.05. In contrast, the S/O = 0.02 of WD 1647+375 falls within the range observed for the comets 67P and Halley, S/O = 0.016–0.08. Overall, the volatile element ratios and high N/O suggest that WD 1647+375 is accreting icy material analogous to KBOs.

The three white dwarfs with published nitrogen detections span a range of compositions and interpretations: WD 1425+540 is thought to accrete a KBO analogue (Xu et al. 2017), G238−44 two distinct planetary bodies, one being an icy KBO analogue and the other being a rocky body (Johnson et al. 2022), and GD378 an icy exo-moon formed in the giant exoplanets' radiation belts (Doyle, Desch

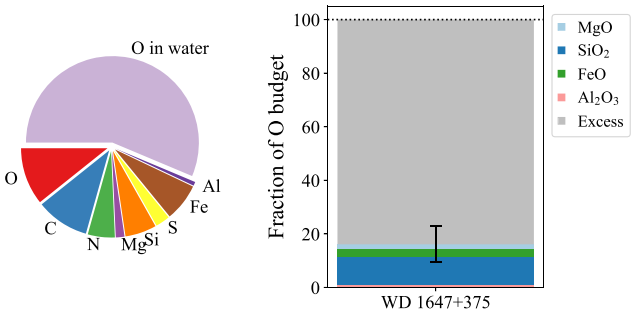

Figure 6. Mass fraction (left) and oxygen budget (right) for the detected heavy elements in WD 1647+375. The error bar represents the total uncertainty on the oxygen budget.

Table 4. Oxygen budget of WD 1647+375.

Component	Fraction of oxygen (per cent)
Al_2O_3	1.0 (0.3)
SiO_2	10.4 (6.0)
FeO	3.1 (1.2)
MgO	1.6 (0.5)
Excess	83.9 (7)

& Young 2021, though recent studies suggest that this hypothesis is unlikely, Trierweiler et al. 2022; Kaiser et al. 2025).

To investigate in more detail the composition of the parent body accreting on to WD 1647+375, we calculated the mass fractions of the detected elements, which are provided in Table 3 and illustrated in Fig. 6. Oxygen is the most abundant element, comprising nearly two-thirds of the total mass. Notably, the volatile nitrogen accounts for ≃5 per cent of the total mass, the highest value among all white dwarfs with nitrogen detections (Xu et al. 2017; Klein et al. 2021; Johnson et al. 2022). This nitrogen abundance is also higher than the values determined for the surface of KBOs and other outer Solar system bodies (Jessberger et al. 1988; Rubin et al. 2019).

Following the prescription of Klein et al. (2010), we calculated the water fraction by evaluating the oxygen budget using the standard stoichiometric ratios within common minerals containing the rock-forming elements Mg, Al, Si, and Fe (Table 4). We considered a scenario similar to that of the bulk Earth – namely that oxygen is primarily bound in MgO, Al_2O_3, SiO_2, and FeO. Since Fe can also be metallic (such as in the Earth's core), we allowed the oxidation state of Fe to vary from being all in the form of FeO to all as metallic. Assuming that all Fe is metallic, we find that excess oxygen is 87 ± 6 per cent. If Fe is entirely locked within FeO, which is a more likely state for a cometary body, the excess oxygen is 84 ± 7 per cent, as shown in the right panel of Fig. 6. This large oxygen excess indicates that the bulk of oxygen was carried as water, and thus the planetary body is rich in water ice. This again supports that WD 1647+375 is accreting an icy exoplanetesimal.

The water-to-rock ratio is a crucial parameter to constrain the interior structure, composition, and formation history of ice-rich planetary bodies (Vazan, Sari & Kessel 2022). From Table 5, the mass fraction of Mg, Al, Si, and Fe, representative of the rocky material in WD 1647+375, constitutes ≈15 per cent. From the oxygen budget calculated above, 83.9 per cent are associated with the accretion of water, and 16.1 per cent were accreted in the form of minerals. Consequently, the mass fraction of oxygen contained in either water or minerals is 56.4 per cent and 10.7 per cent, respectively. The mass

Table 5. Water and rock mass fraction of icy body accreted by WD 1647+375.

Component	Mass fraction (per cent)
Metals (Mg, Al, Si, Fe)	15.2 (3.7)
O in oxides	10.7 (1.1)
O in water (H_2O)	56.4 (5.5)
H in water[a]	7.1 (0.7)
Total H_2O	63.5 (5.6)
Total rock (metal+oxide)	25.9 (3.9)

[a]As the atmosphere of WD 1647+375 is composed of hydrogen, our observations are not sensitive to the accretion of this element, and therefore it is not included in the mass fractions of the *detected* elements in Table 3. The overall mass fractions including C, N, and S (from Table 3) with the above estimates (excluding H in water) amounts to 100 per cent.

fraction of rock is hence the sum of the oxygen and Mg, Al, Si, and Fe mass fractions, i.e. 25.9 per cent. Accounting for the mass fraction of hydrogen associated with the accreted water, 7.1 per cent, results in a water mass fraction of 63.5 per cent, and finally in a water-to-rock ratio 2.45 ± 0.43. This ratio is around six times higher compared to the KBOs in our Solar system that appear to have water-to-rock ratios of 0.43 (Bierson & Nimmo 2019).

3.2 The nature of the planetary body

The bulk composition and mass distribution of elements detected in the atmosphere of WD 1647+375 demonstrate that the accreted object is either a comet or a fragment of the surface of an icy dwarf planet similar to Pluto (Biver et al. 2018). The observed nitrogen enhancement, relative to typical comets, supports the latter scenario, as it can be explained if the accreted material constitutes the mantle and crust of a dwarf planet in a Kuiper belt location. WD 1647+375 is accreting at a rate $\approx 2 \times 10^8\,\mathrm{g\,s^{-1}}$ for at least 13 yrs (spanned by our observations). Assuming a water-like density of $\rho = 1\,\mathrm{g\,cm^{-3}}$ gives firm lower limits on the mass (7.7×10^{16} g) and radius (2.6 km) of the parent body accreting on to the star. If we assume that the accretion phase lasts for 10^5–10^6 yr, as estimated from statistical studies of white dwarfs with infrared dust disks (Girven et al. 2012; Cunningham et al. 2021, 2025)[2], the parent body would be much larger with a mass of $\sim 6 \times 10^{20\text{–}21}$ g and a radius of about $\simeq$50–100 km. These values are large compared to Solar system comets (e.g. Hale–Bopp's mass is $\sim 10^{19}$ g), but would be typical for a KBO. On the other hand, a shorter accretion phase of $\sim 10^4$ yr would permit a body more comet-like in its mass.

In the context of the origin of this planetary object, it is interesting to note that the discussions of white dwarfs accreting KBO-like objects (Xu et al. 2017; Johnson et al. 2022) implicitly assumed that these bodies were formed in a planetary system around the white dwarf progenitor. However, given that three interstellar comets (1I/Oumuamua, 2I/Borisov, and 3I/ATLAS) were identified in the Solar system within a few years (Meech et al. 2017; Jewitt & Luu 2019; Bolin et al. 2025), a tantalizing possibility is that some white dwarfs may accrete such interstellar comets, rather than their own.

[2]Note that these estimates of the accretion phase duration were derived from the statistical analysis of white dwarfs with dusty per cent circumstellar discs detected in the infrared. It is not evident if the accretion of volatile-dominated material would proceed on the same or similar time-scales.

The likelihood of accreting an interstellar object can be investigated from both dynamical and chemical perspectives.

Dynamically, consider an interstellar comet, composed of many particles, that is initially in a hyperbolic orbit around a white dwarf. This orbit may be changed by non-gravitational decelerations on approach to periastron, assuming that the interstellar object contains volatiles to be released (Veras, Eggl & Gänsicke 2015) as noted in the cometary orbits in the Solar system. Independent of these details, if the comet passes through the white dwarf Roche sphere, which has an approximate radius of $R_{\mathrm{Roche}} = 1\mathrm{R}_\odot$, it will tidally disrupt. This process is similar to the well-studied scenario of stars being tidally disrupted by black holes, where roughly half of the material remains bound, and the other half is ejected (Lacy, Townes & Hollenbach 1982; Rees 1988). Numerical simulations have demonstrated that a similar ratio of bound to ejected material is true for the tidal disruption of solid planetary bodies (Veras et al. 2014b; Malamud & Perets 2020).The resulting tidal disruption of the interstellar object would create a debris disc that eventually is accreted on to the white dwarf over a time-scale t_{disc}. The upper bound of t_{disc} is, as stated above, ∼Myr (Girven et al. 2012; Cunningham et al. 2021, 2025), while the lower bound is poorly constrained (Veras & Heng 2020). Then the expected number of accretion events per white dwarf is $\sim (\pi R_{\mathrm{Roche}}^2) n v t_{\mathrm{disc}}$, where v is the stellar velocity dispersion in the relevant local patch of the Milky Way, and n is the number density of interstellar objects. The values of n and t_{disc} are highly uncertain. However, generating an interstellar object pollution rate of one out of every few hundred white dwarfs can be obtained with reasonable assumptions (e.g. $n = 0.2\,\mathrm{au^{-3}}$; Do, Tucker & Tonry 2018, $t_{\mathrm{disc}} = 10^2$ yr, and $v = 10\,\mathrm{km\,s^{-1}}$). For comparison, Dehnen, Hands & Schönrich (2022) estimate the rate of interstellar bodies hitting the Sun as 17 in 1000 yr.

Alternatively, an interstellar object may be gravitationally captured by the white dwarf (Napier, Adams & Batygin 2021a, b; Dehnen & Hands 2022; Dehnen et al. 2022; Belbruno & Green 2024). Once in the system, the object could experience a combination of non-gravitational forces and close encounters with any existing planets, eventually leading to accretion on to the white dwarf (Bonsor & Wyatt 2012; Wyatt et al. 2017; Marino et al. 2018; Rodet & Lai 2024). However, the capture rate of interstellar objects by a Sun–Jupiter like system is small (∼2 objects per 1000 yr) and can only occur at low incoming speeds (typically $v_\infty \leq 4\,\mathrm{km\,s^{-1}}$; Dehnen et al. 2022).

Chemically, 2I/Borisov has many characteristics of a KBO (Jewitt & Seligman 2023). The nature of 1I/'Oumuamua is less well understood, but is either likely to be a small (diameter < 100 m) fragment of N_2 ice from the surface of an exo-Pluto (Desch & Jackson 2021) or a dark comet arising from the cold and distant regions of the extrasolar system (Seligman et al. 2022). There are similar fragments of crusts of differentiated Pluto-like dwarf planets observed in our Solar system (Biver et al. 2018). For example, the comet C/2016 R2 is thought to sample the N_2 ice-rich crust of a differentiated Pluto-like body, and such larger objects could be expected among comets ejected from stellar systems. Thus, compositionally, interstellar objects are likely to resemble other intrinsic comets, but there is a distinct possibility, based on observations like C/2016R2 in our Solar system, that some interstellar comets could be N_2 rich. The chemical composition of the recently discovered interstellar comet, 3I/ATLAS is not yet sufficiently well-constrained to be discussed within the context of our study of WD 1647+375 (Jewitt et al. 2025; Puzia et al. 2025). Nevertheless, regardless of their actual origin, white dwarfs have the potential

to provide an important tool for measuring the abundances of icy exoplanetesimals.

4 CONCLUSION

The detection of nitrogen alongside other heavy elements indicates that WD 1647+375 is accreting an icy, Kuiper Belt-like body with a large (63.5 per cent) water content. WD 1647+375 is the first hydrogen atmosphere white dwarf confirmed to be purely accreting a KBO analogue, similar to the helium atmosphere white dwarf WD 1425+540. Given the fact that helium-rich atmospheres have sinking time-scales orders of magnitude longer than their hydrogen-rich counterparts, and since their accretion history is therefore often uncertain (Koester 2009; O'Brien et al. 2025), the discovery of WD 1647+375 provides an unambiguous measurement of metal abundances and accretion rates for a planetary body with comet-like composition.

The origin of the body accreting on to WD 1647+375 remains uncertain, and we raise the possibility that it may be of interstellar origin, rather than belonging to a planetary system formed around the progenitor of the white dwarf. The relative probabilities of different scenarios (an intrinsic comet, a KBO fragment, or an interstellar comet) are subject to a number of uncertain parameters, including the fraction of intrinsic comets lost during the (post) main-sequence evolution, and the space density, mass distribution, and lifetime of interstellar comets. It is difficult to distinguish between these scenarios solely from its chemical composition, and it will require more detailed dynamical simulations to explore the likelihood of the different possible origins.

Our study of WD 1647+375 demonstrates the existence of icy exoplanetesimals that could deliver water and other volatiles to terrestrial planets in extrasolar systems – a pre-requisite for the development of life in other worlds. This discovery is based on the far-ultraviolet spectroscopic capabilities of *HST*, emphasizing the importance for future ultraviolet missions in exploring other worlds and the origins of life.

ACKNOWLEDGEMENTS

We thank the anonymous referee for valuable comments. This research is based on observations made with the NASA/ESA Hubble Space Telescope obtained from the Space Telescope Science Institute, which is operated by the Association of Universities for Research in Astronomy, Inc., under NASA contract NAS 5–26555. These observations are associated with programme 12474 and 12869. This reseacrh is based on observations collected at the European Organisation for Astronomical Research in the Southern Hemisphere under ESO programme 115.28GM.001. SS and BTG received funding from the European Research Council under the European Union's Horizon 2020 research and innovation programme number 101002408 (MOS100PC) and 101020057 (WDPLANETS). BTG acknowledges support from the Fundación Occident and the Instituto de Astrofísica de Canarias under the Visiting Researcher Programme 2022–2025 agreed between both institutions.

DATA AVAILABILITY

The COS spectroscopy data underlying this paper are available in the raw form via the *HST* MAST archive under the programs 12474 and 12869. The X-shooter spectra from VLT is available in ESO archive under the programme 115.28GM.001.

REFERENCES

Anders E., 1989, Nature, 342, 255
Anslow R. J., Bonsor A., Rimmer P. B., 2023, Proc. R. Soc. A, 479, 20230434
Barrett T. J., Bryson J. F. J., Geraki K., 2025, Icarus, 436, 116588
Belbruno E., Green J., 2024, Celest. Mech. Dyn. Astron., 136, 52
Bierson C. J., Nimmo F., 2019, Icarus, 326, 10
Biver N. et al., 2018, A&A, 619, A127
Bodewits D. et al., 2020, Nat. Astron., 4, 867
Bolin B. T. et al., 2025, MNRAS, 542, L139
Bonsor A., Wyatt M. C., 2012, MNRAS, 420, 2990
Bourrier V. et al., 2018, A&A, 615, A117
Brouwers M. G., Buchan A. M., Bonsor A., Malamud U., Lynch E., Rogers L., Koester D., 2023, MNRAS, 519, 2663
Cunningham T. et al., 2021, MNRAS, 503, 1646
Cunningham T. et al., 2025, MNRAS, 539, 2021
DESI Collaboration, 2025, preprint (arXiv:2503.14745)
Debes J. H., 2006, ApJ, 652, 636
Dehnen W., Hands T. O., 2022, MNRAS, 512, 4062
Dehnen W., Hands T. O., Schönrich R., 2022, MNRAS, 512, 4078
Desch S. J., Jackson A. P., 2021, J. Geophys. Res. (Planets), 126, e06807
Do A., Tucker M. A., Tonry J., 2018, ApJ, 855, L10
Doyle A. E., Desch S. J., Young E. D., 2021, ApJ, 907, L35
Doyle A. E. et al., 2023, ApJ, 950, 93
Dufour P., Blouin S., Coutu S., Fortin-Archambault M., Thibeault C., Bergeron P., Fontaine G., 2017, in Tremblay P.-E., Gänsicke B. T., Marsh T. R., eds, ASP Conf. Ser. Vol. 509, 20th European Workshop on White Dwarfs. Astron. Soc. Pac., San Francisco, p. 3
Farihi J., Barstow M. A., Redfield S., Dufour P., Hambly N. C., 2010, MNRAS, 404, 2123
Farihi J., Gänsicke B. T., Koester D., 2013, Science, 342, 218
Gaia Collaboration, 2023, A&A, 674, A1
Gänsicke B. T., Koester D., Farihi J., Girven J., Parsons S. G., Breedt E., 2012, MNRAS, 424, 333
Gentile Fusillo N. P., Gänsicke B. T., Farihi J., Koester D., Schreiber M. R., Pala A. F., 2017, MNRAS, 468, 971
Gianninas A., Bergeron P., Ruiz M. T., 2011, ApJ, 743, 138
Girven J., Brinkworth C. S., Farihi J., Gänsicke B. T., Hoard D. W., Marsh T. R., Koester D., 2012, ApJ, 749, 154
Hollands M. A., Koester D., Alekseev V., Herbert E. L., Gänsicke B. T., 2017, MNRAS, 467, 4970
Hollands M. A. et al., 2020, Nat. Astron., 4, 663
Izquierdo P., Toloza O., Gänsicke B. T., Rodríguez-Gil P., Farihi J., Koester D., Guo J., Redfield S., 2021, MNRAS, 501, 4276
Jackson A. P., Desch S. J., 2021, J. Geophys. Res. (Planets), 126, e06706
Jessberger E. K., Christoforidis A., Kissel J., 1988, Nature, 332, 691
Jewitt D., Luu J., 2019, ApJ, 886, L29
Jewitt D., Seligman D. Z., 2023, ARA&A, 61, 197
Jewitt D., Hui M.-T., Mutchler M., Kim Y., Agarwal J., 2025, ApJL, 990, 1
Johnson T. M., Klein B. L., Koester D., Melis C., Zuckerman B., Jura M., 2022, ApJ, 941, 113
Jura M., 2003, ApJ, 584, L91
Kaiser B. C., Clemens J. C., Blouin S., Dennihy E., Dufour P., Hegedus R. J., Reding J. S., 2025, ApJ, 979, 111
Kausch W. et al., 2015, A&A, 576, A78
Kawka A., Vennes S., 2012, A&A, 538, A13
Kiefer F., Lecavelier des Etangs A., Boissier J., Vidal-Madjar A., Beust H., Lagrange A. M., Hébrard G., Ferlet R., 2014a, Nature, 514, 462
Kiefer F., Lecavelier des Etangs A., Augereau J. C., Vidal-Madjar A., Lagrange A. M., Beust H., 2014b, A&A, 561, L10
Klein B., Jura M., Koester D., Zuckerman B., Melis C., 2010, ApJ, 709, 950
Klein B. L., Doyle A. E., Zuckerman B., Dufour P., Blouin S., Melis C., Weinberger A. J., Young E. D., 2021, ApJ, 914, 61
Koester D., 2009, A&A, 498, 517
Koester D., 2010, Mem. Soc. Astron. Italiana, 81, 921
Koester D., Gänsicke B. T., Farihi J., 2014, A&A, 566, A34
Koester D., Kepler S. O., Irwin A. W., 2020, A&A, 635, A103
Kral Q., Huet P., Bergez-Casalou C., Thébault P., Charnoz S., Fornasier S., 2024, A&A, 692, A70
Lacy J. H., Townes C. H., Hollenbach D. J., 1982, ApJ, 262, 120

Lodders K., 2003, ApJ, 591, 1220
Malamud U., Perets H. B., 2016, ApJ, 832, 160
Malamud U., Perets H. B., 2020, MNRAS, 492, 5561
Marino S., Bonsor A., Wyatt M. C., Kral Q., 2018, MNRAS, 479, 1651
McDonough W. F., Sun S. s., 1995, Chem. Geol., 120, 223
Meech K. J. et al., 2017, Nature, 552, 378
Melis C., Dufour P., 2017, ApJ, 834, 1
Napier K. J., Adams F. C., Batygin K., 2021a, Planet. Sci., 2, 53
Napier K. J., Adams F. C., Batygin K., 2021b, Planet. Sci., 2, 217
O'Brien M. W., Tremblay P.-E., Klein B. L., Melis C., Koester D., Buchan A. M., Veras D., Doyle A. E., 2025, MNRAS, 539, 171
Oliverira C., Beland S., Keyes C. T., Aloisi A., Niemi S., Osterman S., Proffitt C., 2010, in Deustua S., Oliveira C.eds, STScI Calibration Workshop, conf. proc. Hubble after SM4. Preparing JWST. p. 45
Paganini L., Mumma M. J., Villanueva G. L., DiSanti M. A., Bonev B. P., Lippi M., Boehnhardt H., 2012, ApJ, 748, L13
Piani L., Marrocchi Y., Rigaudier T., Vacher L. G., Thomassin D., Marty B., 2020, Science, 369, 1110
Puzia T. H., Rahatgaonkar R., Carvajal J. P., Nayak P. K., Luco B., 2025, preprint (arXiv:2508.02777)
Raddi R., Gänsicke B. T., Koester D., Farihi J., Hermes J. J., Scaringi S., Breedt E., Girven J., 2015, MNRAS, 450, 2083
Rees M. J., 1988, Nature, 333, 523
Rodet L., Lai D., 2024, MNRAS, 527, 11664
Rogers J. G., Dorn C., Aditya Raj V., Schlichting H. E., Young E. D., 2025, ApJ, 979, 79
Rubin M. et al., 2019, MNRAS, 489, 594
Sahu S. et al., 2023, MNRAS, 526, 5800
Schatzman E., 1945, Ann. d'Astrophysique, 8, 143
Seligman D. Z. et al., 2022, Planet. Sci., 3, 150
Stone N., Metzger B. D., Loeb A., 2015, MNRAS, 448, 188
Strøm P. A. et al., 2020, PASP, 132, 101001
Trierweiler I. L., Doyle A. E., Melis C., Walsh K. J., Young E. D., 2022, ApJ, 936, 30
Vazan A., Sari R., Kessel R., 2022, ApJ, 926, 150
Veras D., Heng K., 2020, MNRAS, 496, 2292
Veras D., Shannon A., Gänsicke B. T., 2014a, MNRAS, 445, 4175
Veras D., Leinhardt Z. M., Bonsor A., Gänsicke B. T., 2014b, MNRAS, 445, 2244
Veras D., Eggl S., Gänsicke B. T., 2015, MNRAS, 452, 1945
Vernet J. et al., 2011, A&A, 536, A105
Walters N., Farihi J., Marsh T. R., Breedt E., Cauley P. W., von Hippel T., Hermes J. J., 2023, MNRAS, 519, 1381
Welsh B. Y., Montgomery S. L., 2018, MNRAS, 474, 1515
Williams J. T., Gänsicke B. T., Swan A., O'Brien M. W., Izquierdo P., Cutolo A. M., Cunningham T., 2024, A&A, 691, A352
Williams J. T. et al., 2025, MNRAS, 541, 1377
Wilson D. J., Gänsicke B. T., Farihi J., Koester D., 2016, MNRAS, 459, 3282
Wilson T. G., Farihi J., Gänsicke B. T., Swan A., 2019, MNRAS, 487, 133
Wyatt M. C., Bonsor A., Jackson A. P., Marino S., Shannon A., 2017, MNRAS, 464, 3385
Xu S., Zuckerman B., Dufour P., Young E. D., Klein B., Jura M., 2017, ApJ, 836, L7
Young E. D., Shahar A., Schlichting H. E., 2023, Nature, 616, 306
Zhou W.-H., Liu S.-F., Lin D. N. C., 2024, A&A, 687, A107
Zuckerman B., Koester D., Reid I. N., Hünsch M., 2003, ApJ, 596, 477
Zuckerman B., Koester D., Melis C., Hansen B. M., Jura M., 2007, ApJ, 671, 872

APPENDIX A: ANALYSIS OF THE SNAPSHOT SPECTRUM

The airglow correction (Fig. A1) and abundance analysis (Fig. A2) for the snapshot spectra of WD 1647+375 was performed following the same procedure as for the deeper exposure, see Section 2 in the main text for details.

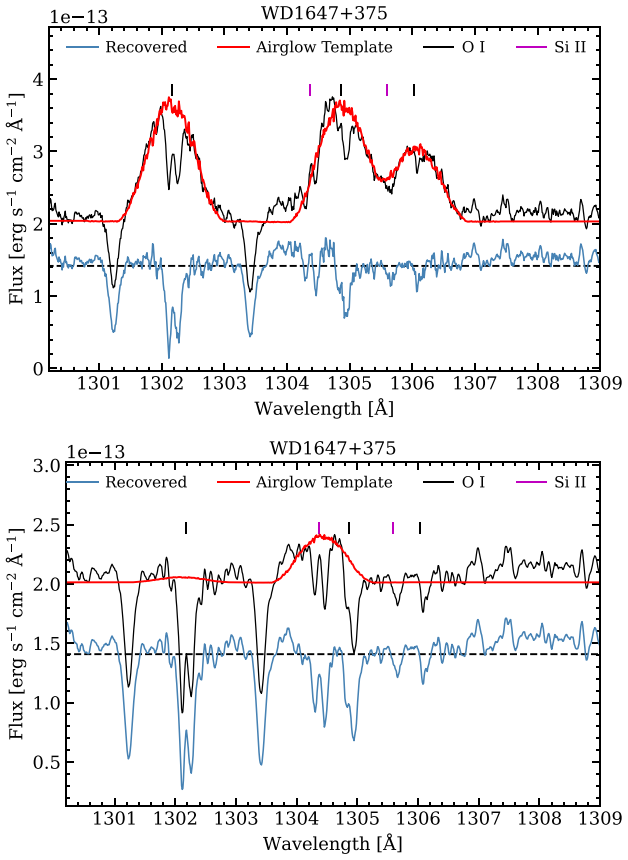

Figure A1. Airglow correction of the snapshot spectrum of WD 1647+375 where the raw and airglow fitted template spectra are shown in solid black and red lines, respectively. The initial fit (top panel) partially removed the airglow feature in the spectral region 1304−1305 Å. Therefore, a second fit (bottom panel) was applied to the output of the first correction to get the final spectra for abundance analysis. For more description, refer Fig. 1.`

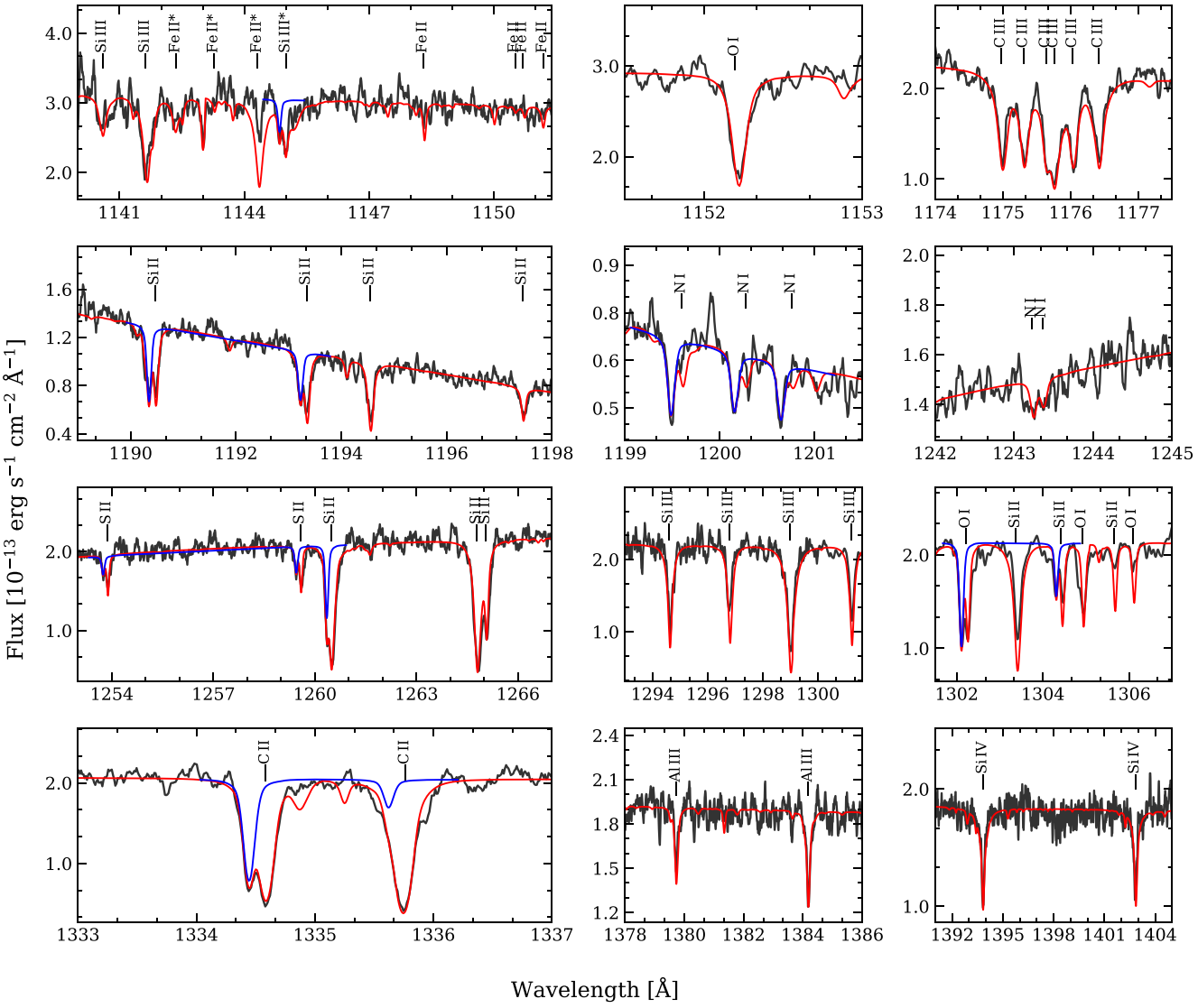

Figure A2. The airglow-corrected *HST* COS snapshot spectrum of WD 1647+375 (black) and the best-fitting model (red) with the line velocities from Table 1 and the weighted average abundances from Table 3. Since we have plotted the average abundances, the individual fits to the Si lines look poor. The ISM lines are fitted with a Gaussian profile and are shown in blue. Several transitions of C, N, O, S, Si, Al, and Fe are labelled, where ∗ denotes a blend of Si with Fe lines.

This paper has been typeset from a TEX/LATEX file prepared by the author.